

Unifying formalism and closures for coarse-grained approaches to turbulence

A. Cimarelli¹†, N. Marras¹, B. Niceno² and Y. Tessier Urrecha¹

¹Department of Engineering "Enzo Ferrari", University of Modena and Reggio Emilia, 41125 Modena, Italy

²Paul Scherrer Institute, ETH, 5232 Villigen, Switzerland

(Received xx; revised xx; accepted xx)

We propose the use of an unifying paradigm for the assessment and development of closed forms of the coarse-grained Navier-Stokes equations in approaches ranging from the statistical to the scale-resolving ones. It consists in the exact formalism provided by the temporally filtered Navier-Stokes equations. The fundamental idea is that the smoothing action of turbulent stresses can be described as a temporal filtering operator implicitly applied to the solution. Contrary to the average and spatial filtering operators, the temporal filter is an unifying operator smoothly varying within the statistical and scale-resolving realms. The potential of the temporal filtering paradigm is here highlighted by unveiling relevant algebraic properties and by deriving a new class of turbulence closures. A dynamic procedure is derived and shown to provide an unifying closure for both scale-resolving and statistical approaches. Results show that an improved physics is captured. Challenging phenomena such as the laminar to turbulence transition and the dependence of separation and reattachment on free-stream turbulence applied through boundary conditions are captured.

Key words: Coarse-grained approaches to turbulence, Turbulence closures

1. Introduction

The more classical coarse-grained approach to the Navier-Stokes equations is that provided by the Reynolds-averaged Navier-Stokes equations (RANS). In their derivation an ensemble average operator $\langle \cdot \rangle$ is adopted. Associated with this operator is the appearance in the momentum equations of the Reynolds stresses which, accordingly, can be understood as second-order statistical moments of the velocity field,

$$R(u_i, u_j) = \langle u_i u_j \rangle - \langle u_i \rangle \langle u_j \rangle \quad (1.1)$$

Because of the Reynolds stresses, the system of equations is however not closed thus posing the question on how to close the system (Wilcox *et al.* 1998). The most classical way is to consider a gradient hypothesis such that the turbulent transport of mean momentum goes down the mean velocity gradient, the so-called Boussinesq hypothesis of eddy viscosity. Clearly, the solution is not anymore the solution of the exact RANS equations but of a different set of equations that depends on the model used for the turbulent stresses. This set of equations will be hereafter called modeled RANS equations. Accordingly, their solution cannot be anymore interpreted as the ensemble average

† Email address for correspondence: andrea.cimarelli@unimore.it

solution of the Navier-Stokes equations. As a matter of facts, it is well known that classical turbulence closures predict unsteady solutions in flow problems with a large separation of scales whose ensemble solutions are on the contrary steady. Depending on the additional transport of momentum introduced by the turbulence closure, the solution gets different statistical features that are not present in the ensemble average. Thus, one might conclude that the solutions of the modeled equations are simply wrong. However, an alternative interpretation could be equivalently valid. Indeed, it is also possible to think that this discrepancy in the solutions is a symptom of the fact that the modeled equations represent a coarse-grained approach whose paradigm is different from that provided by the exact RANS equations. In other words, the reference for the solutions of the modeled RANS equations cannot be anymore the exact RANS solution and any discrepancies do not necessarily lead to the conclusion that the solutions of the modeled equations are wrong. If that is the case, the question is: is it possible to define a general formalism able to characterize the different types of coarse-grained approaches established by the different turbulence closures? Can this formalism be used to improve turbulence closures? These questions are even more relevant when considering hybrid turbulence closures where scale-resolving models typical of Large Eddy Simulation (LES) are combined with statistical models typical of RANS. The resulting coarse-grained approach is an ambiguous combination of statistical and scale-resolving methods that again lacks a general exact formalism able to describe them simultaneously.

In the present work, we propose the use of an unifying paradigm able to simultaneously describe both statistical and scale-resolving methods for the coarse-grained solution of the Navier-Stokes equations. The potential of the proposed formalism is demonstrated by the derivation of a new class of dynamic turbulence closures able to address solution features typical of both scale-resolving and statistical methods.

The paper is organized as follows. The theoretical framework is introduced in section §2. A family of improved turbulence closures is described in section §3. Tests are performed for a transitional flow over a rounded leading-edge flat plate. The numerical settings and the flow setup are outlined in section §4 while the results from scale-resolving and statistical simulations are reported in sections §5 and §6, respectively. The paper is closed by concluding remarks in section §7 and by two appendices further assessing the improved turbulence closures, sections §A and §B.

2. Theoretical framework

The funding aspect of the present work is the use of an operatorial approach for the description of the smoothing action given by the additional momentum transport introduced by turbulence models commonly employed in RANS and hybrid LES/RANS approaches. The basic assumption is that the smoothing action of the turbulence closure can be modeled as a temporal filter operator implicitly applied to the Navier-Stokes equations. This operator is hereafter denoted as $\langle \cdot \rangle_\tau$, where τ represents the filter time scale implicitly imposed by the turbulence closure. This operatorial assumption suggests that the modeled equations commonly solved in RANS and hybrid LES/RANS approaches can be better studied within the exact framework provided by the temporally filtered Navier-Stokes equations,

$$\left. \begin{aligned} \frac{\partial \langle u_i \rangle_\tau}{\partial x_i} &= 0 \\ \frac{\partial \langle u_i \rangle_\tau}{\partial t} + \frac{\partial \langle u_i \rangle_\tau \langle u_j \rangle_\tau}{\partial x_j} &= -\frac{1}{\rho} \frac{\partial \langle p \rangle_\tau}{\partial x_i} + \nu \frac{\partial^2 \langle u_i \rangle_\tau}{\partial x_j \partial x_j} - \frac{\partial R_\tau(u_i, u_j)}{\partial x_j} \end{aligned} \right\} \quad (2.1)$$

where $R_\tau(u_i, u_j)$ represents the tensor of turbulent stresses that in the modeled RANS and LES/RANS equations is provided by the turbulence closure. To note that in the temporally filtered Navier-Stokes equations (2.1), we have assumed that the temporal filtering operator commutes with the temporal derivative. In other words, we have assumed that the filter time scale implicitly induced by the turbulence closure is constant in time.

Before addressing the closure issue and its relation with the temporal filtering operator, it is important to address first the theoretical framework provided by the temporally filtered Navier-Stokes equations in their exact form. To note that this framework has already attracted some interest in the scientific community. The reader is referred to the works Pruett *et al.* (2003), Pruett (2008) and references therein for a detailed assessment of the temporally filtered framework. Here, we report the main properties that are of relevance for the present work. In the framework provided by the temporally filtered Navier-Stokes equations (2.1), the turbulent stress tensor takes the exact form,

$$R_\tau(u_i, u_j) = \langle u_i u_j \rangle_\tau - \langle u_i \rangle_\tau \langle u_j \rangle_\tau \quad (2.2)$$

and the time filtering operator is not implicitly induced by the smoothing action of the turbulence closure, rather is explicitly applied. For a generic quantity β , the explicit filter operator can be formally and quite generally expressed as a convolution integral (Leonard 1975),

$$\langle \beta(\mathbf{x}, t) \rangle_\tau = \int \beta(\mathbf{x}, t') G(t - t', \tau) dt' \quad (2.3)$$

where G is a filter kernel with characteristic time scale τ that we assume constant preserving,

$$\int G(t - t', \tau) dt' = 1 \quad (2.4)$$

As already shown by previous pivotal works like those carried out by Fadai-Ghotbi *et al.* (2010), Friess *et al.* (2015) and Duffal *et al.* (2022), a peculiar and relevant aspect of the exact formalism provided by the temporally filtered Navier-Stokes equations is the direct link between the scale-resolving and the statistical approaches. Indeed, from a point of view of operators we have that the ensemble average is asymptotically recovered by the temporal filter $\langle \cdot \rangle_\tau = \langle \cdot \rangle$ when $\tau U/L \gg 1$ with U and L the characteristic velocity and length scales of the problem, provided that the flow has a statistically steady solution (Kampé de Fériet & Betchov 1951). This asymptotic link between the scale-resolving and statistical approaches is recovered also by the solution of the temporally filtered Navier-Stokes equations (2.1). Indeed, when $\tau U/L \gg 1$ the exact turbulent stresses reduce to the exact Reynolds stresses, $R_\tau(u_i, u_j) = R(u_i, u_j)$ because $\langle u_i u_j \rangle_\tau - \langle u_i \rangle_\tau \langle u_j \rangle_\tau = \langle u_i u_j \rangle - \langle u_i \rangle \langle u_j \rangle$, hence the solution of the temporally filtered Navier-Stokes equations (2.1) converges to the solution of the exact RANS equations, namely $\langle u_i \rangle_\tau = \langle u_i \rangle$. In other words, the temporally filtered Navier-Stokes equations represent an unifying theoretical framework able to describe the behaviour of solutions from turbulence closures ranging from the scale-resolving to the statistical approach. This property is missed by the exact spatially filtered Navier-Stokes equations and by the exact RANS equations that can describe only the scale-resolving and the statistical approaches separately. The aim of the present work is to support this change of paradigm by showing how and to what degree the temporal filtering formalism can be used to assess and eventually improve turbulence closures commonly adopted to solve the modeled RANS and hybrid LES/RANS equations.

A relevant aspect of the use of the temporal filtering approach is given by the fact that

some important algebraic properties can be leveraged by considering different filtering operators hierarchically organized at multiple levels (Germano 1992). In particular, by introducing a second filter operator with a larger characteristic time scale $T > \tau$, it is possible to evaluate the turbulent stresses at a coarser level as

$$R_{T\tau}(u_i, u_j) = \langle\langle u_i u_j \rangle_\tau \rangle_T - \langle\langle u_i \rangle_\tau \rangle_T \langle\langle u_j \rangle_\tau \rangle_T \quad (2.5)$$

These turbulent stresses are related with those at the finer level as

$$R_{T\tau}(u_i, u_j) = \langle R_\tau(u_i, u_j) \rangle_T + \langle\langle u_i \rangle_\tau \langle u_j \rangle_\tau \rangle_T - \langle\langle u_i \rangle_\tau \rangle_T \langle\langle u_j \rangle_\tau \rangle_T \quad (2.6)$$

thus allowing us to write the following exact equation

$$R_{T\tau}(u_i, u_j) - \langle R_\tau(u_i, u_j) \rangle_T = \langle\langle u_i \rangle_\tau \langle u_j \rangle_\tau \rangle_T - \langle\langle u_i \rangle_\tau \rangle_T \langle\langle u_j \rangle_\tau \rangle_T \quad (2.7)$$

which is the temporal analogue of one of the most famous identities in turbulence (Germano 1992). This exact algebraic relation is exploited here for the first time to derive a general approach for improving turbulence closures commonly adopted in RANS and hybrid LES/RANS approaches.

3. Improved RANS turbulence closures

The basic assumption of the present work is that the smoothing action of the additional momentum transport induced by turbulence closures can be modeled as an implicit filtering of the flow solution at a time scale τ that, without loss of generality, can be estimated as

$$\tau = \sqrt{\frac{\nu + \nu_\tau}{\epsilon}} \quad (3.1)$$

where ν_τ is the eddy viscosity associated with the turbulence closure while ϵ is the dissipation rate of kinetic energy. Accordingly, the solution from turbulence closures is expected to reduce to a statistically steady state when $\tau U/L \gg 1$. In this case, the reference framework is that provided by the exact RANS equations or equivalently by the large time scale limit of the temporally filtered Navier-Stokes equations. On the other hand, for flow cases characterized by a large separation of scales, the solution from turbulence closures is usually able to capture some unsteadiness since $\tau U/L \leq 1$. In this condition, the paradigm for turbulence closures is no longer that provided by the exact RANS equations, rather only the exact framework provided by the temporally filtered Navier-Stokes equations can be used. Hence, this change of paradigm describes both the statistical and scale-resolving features of the solutions from turbulence closures and opens the possibility of improving them. The use of identity (2.7) and of the related decomposition of the velocity field at two filter levels τ and T , is a sound starting point to reach this goal.

3.1. Dynamic RANS closure

In the context of turbulence closures and, hence, of the modeled temporally filtered Navier-Stokes equations, the decomposition of the solution at two filter levels suggested by the identity (2.7) takes the following interpretation. The first filter operator at the time scale τ should be understood as implicitly applied by the eddy viscosity of the closure itself. Hence, all the quantities hereafter formally reported under the first filter operator $\langle \cdot \rangle_\tau$ actually represent quantities that are simply resolved. On the contrary, the second filter operator $\langle \cdot \rangle_T$ is the only explicitly filtering operation performed at a time scale $T > \tau$.

The formally exact algebraic relation (2.7), requires to model turbulent stresses at the resolved and test filter level, $R_\tau(u_i, u_j)$ and $R_T(u_i, u_j)$ respectively. The classical approach to model the turbulent stresses is to consider the Boussinesq gradient hypothesis by which the momentum is assumed to flow down the resolved velocity gradient. By applying this assumption we can write

$$\begin{aligned} R_\tau(u_i, u_j) &= -2\nu_\tau \langle S_{ij} \rangle_\tau \\ R_{T_\tau}(u_i, u_j) &= -2\nu_{T_\tau} \langle \langle S_{ij} \rangle_\tau \rangle_T \end{aligned} \quad (3.2)$$

where $S_{ij} = (\partial u_i / \partial x_j + \partial u_j / \partial x_i) / 2$ is the rate of deformation tensor and the two diffusion coefficients, ν_τ and ν_{T_τ} , are the eddy viscosity associated to the two filter levels. The latter are commonly modeled through turbulent quantities obtained from dedicated evolution equations (Wilcox *et al.* 1998). Without loss of generality, let us consider as evolved turbulent quantities, the turbulent kinetic energy and dissipation of the decomposed field,

$$\begin{aligned} \nu_\tau &= c_\mu \frac{k_\tau^2}{\epsilon_\tau} \\ \nu_{T_\tau} &= c_\mu \frac{k_{T_\tau}^2}{\epsilon_{T_\tau}} \end{aligned} \quad (3.3)$$

where c_μ is usually a constant coefficient and is assumed here to be the same for the two solutions at the two filter levels (Meneveau & Katz 2000). Here, k_τ and ϵ_τ are the turbulent kinetic energy and turbulent dissipation associated with the resolved flow solution $\langle \mathbf{u} \rangle_\tau$ and are computed through their transport equations. Again, without loss of generality such equations can be of the following form,

$$\left. \begin{aligned} \frac{\partial k_\tau}{\partial t} + \frac{\partial k_\tau \langle u_j \rangle_\tau}{\partial x_j} &= 2\nu_\tau \langle S_{ij} \rangle_\tau \langle S_{ij} \rangle_\tau - \epsilon_\tau + \frac{\partial}{\partial x_j} \left[\left(\nu + \frac{\nu_\tau}{\sigma^k} \right) \frac{\partial k_\tau}{\partial x_j} \right] \\ \frac{\partial \epsilon_\tau}{\partial t} + \frac{\partial \epsilon_\tau \langle u_j \rangle_\tau}{\partial x_j} &= \frac{\epsilon_\tau}{k_\tau} \left(2C_{\epsilon_1} \nu_\tau \langle S_{ij} \rangle_\tau \langle S_{ij} \rangle_\tau - C_{\epsilon_2} \epsilon_\tau \right) + \frac{\partial}{\partial x_j} \left[\left(\nu + \frac{\nu_\tau}{\sigma^\epsilon} \right) \frac{\partial \epsilon_\tau}{\partial x_j} \right] \end{aligned} \right\} \quad (3.4)$$

where σ^k , σ^ϵ , C_{ϵ_1} and C_{ϵ_2} are adjustable model coefficients (Launder & Spalding 1983). On the other hand, k_{T_τ} and ϵ_{T_τ} are the turbulent kinetic energy and turbulent dissipation associated with the flow solution at the second filter level $\langle \langle \mathbf{u} \rangle \rangle_T$. These latter are not transported, rather can be computed as

$$\begin{aligned} k_{T_\tau} &= \langle k_\tau \rangle_T + \mathcal{L}_{ii}/2 \\ \epsilon_{T_\tau} &= \langle \epsilon_\tau \rangle_T + \nu \mathcal{D}_{ii} \end{aligned} \quad (3.5)$$

where the tensors \mathcal{L}_{ij} and \mathcal{D}_{ij} take origin from the same algebraic property introduced by the use of filtering formalism when comparing hierarchically organized filter levels. In particular, \mathcal{L}_{ij} directly comes from identity (2.7),

$$\mathcal{L}_{ij} \equiv R_T(u_i, u_j) - \langle R_\tau(u_i, u_j) \rangle_T = \langle \langle u_i \rangle_\tau \langle u_j \rangle_\tau \rangle_T - \langle \langle u_i \rangle_\tau \rangle_T \langle \langle u_j \rangle_\tau \rangle_T \quad (3.6)$$

on the other hand, \mathcal{D}_{ij} derives from the same arguments but applied to the velocity gradient,

$$\begin{aligned} \mathcal{D}_{ij} &\equiv R_T \left(\frac{\partial u_i}{\partial x_j}, \frac{\partial u_i}{\partial x_j} \right) - \left\langle R_\tau \left(\frac{\partial u_i}{\partial x_j}, \frac{\partial u_i}{\partial x_j} \right) \right\rangle_T = \\ &\left\langle \frac{\partial \langle u_i \rangle_\tau}{\partial x_j} \frac{\partial \langle u_i \rangle_\tau}{\partial x_j} \right\rangle_T - \frac{\partial \langle \langle u_i \rangle_\tau \rangle_T}{\partial x_j} \frac{\partial \langle \langle u_i \rangle_\tau \rangle_T}{\partial x_j} \end{aligned} \quad (3.7)$$

All the arguments are now in place to exploit identity (2.7) for the development of a generic framework for the improvement of turbulence closures. By substituting modeling assumptions (3.3) into the Boussinesq hypothesis (3.2), the identity (2.7) can be rewritten as

$$2c_\mu \left\langle \frac{k_\tau^2}{\epsilon_\tau} \langle S_{ij} \rangle_\tau \right\rangle_T - 2c_\mu \frac{k_{T\tau}^2}{\epsilon_{T\tau}} \langle \langle S_{ij} \rangle_\tau \rangle_T = \langle \langle u_i \rangle_\tau \langle u_j \rangle_\tau \rangle_T - \langle \langle u_i \rangle_\tau \rangle_T \langle \langle u_j \rangle_\tau \rangle_T \quad (3.8)$$

that in a more compact form reads

$$c_\mu \mathcal{M}_{ij} = \mathcal{L}_{ij} \quad (3.9)$$

where

$$\mathcal{M}_{ij} = 2 \left\langle \frac{k_\tau^2}{\epsilon_\tau} \langle S_{ij} \rangle_\tau \right\rangle_T - 2 \frac{k_{T\tau}^2}{\epsilon_{T\tau}} \langle \langle S_{ij} \rangle_\tau \rangle_T \quad (3.10)$$

In equations (3.9) the only unknown is the model coefficient c_μ that can be easily computed as the value that minimizes the mean square error of the system (Lilly 1992),

$$c_\mu = \frac{\mathcal{M}_{ij} \mathcal{L}_{ij}}{\mathcal{M}_{ij} \mathcal{M}_{ij}} \quad (3.11)$$

Equation (3.11) represents a new class of turbulence closures. Indeed, the tensor \mathcal{M}_{ij} has been derived here specifically for the $k - \epsilon$ model but can be equivalently written for any other two-equation eddy viscosity model. This new class of models (3.11) will be hereafter called dynamic RANS closures. To note that this procedure is similar to that pursued in Large-Eddy Simulation (LES) (Germano *et al.* 1991) and in hybrid approaches such as Detached eddy simulation (DES) (Yin *et al.* 2015). The main difference is given by the fact that the new dynamic RANS approach is based on the temporal filtering formalism and aims at improving the predictions of both statistical and scale-resolving approaches typical of RANS and hybrid LES/RANS solutions.

3.2. Foreseen applications

The dynamic procedure developed for the evaluation of the model coefficient c_μ is based on the paradigm provided by the temporally filtered Navier-Stokes equations and on turbulence closures commonly employed in the modeled RANS equations. These are two key aspects for the developed coarse-grained approach. Indeed, from one side we have that the dynamic procedure explicitly pursues the temporal filtering formalism thus enabling a scale-resolving flow solution when the spatial and temporal resolution allow it. From the other side, we have that the baseline turbulence closure is a RANS model thus enabling, together with the large time-scale limit of the temporally filtered equations, a statistical flow solution when the spatial and temporal resolution is too coarse. In other words, the developed dynamic RANS approach represents an unifying closure with the potential of improving predictions of flow solutions ranging from the steady-state statistical to the unsteady scale-resolving ones, depending on the numerical settings adopted.

In light of the above arguments, the target of the developed dynamic RANS approach is to improve the practice in very-coarse simulations such as those commonly adopted in real-world CFD applications, namely steady-state statistical RANS and unsteady scale-resolving hybrid LES/RANS approaches. In particular, we foresee two main areas where the developed dynamic procedure is expected to provide a significant contribution. 1) Improvement of the accuracy of the solution with respect to classical RANS closures when adopting very coarse-grained and steady-state numerical settings. 2) Unlocking more

accurate scale-resolving features than traditional hybrid LES/RANS approaches when the grid and spatial resolution allow them to be developed in coarse-grained unsteady numerical settings. As far as it concerns the latter, we foresee an improved ability in capturing laminar to turbulence transitional phenomena and in the responsiveness to changes in the free-stream turbulence boundary conditions. All these aspects will be quantitatively addressed through numerical simulations in the following sections.

4. Transitional flow over a rounded leading-edge flat plate

The present section reports the first attempt to assess the properties of the proposed dynamic procedure. Different flow cases have been considered, such as the flow around a rectangular cylinder and the flow over a bump which are reported in appendix §A and §B, respectively. Here, we focus on the transitional flow over a rounded leading edge flat plate under different free-stream turbulence conditions, the so-called T3L test case series of the ERCOFTAC suite (Yang & Voke 2001; Bassi *et al.* 2020; Cimarelli *et al.* 2020). The T3L case is chosen because it explicitly concerns flow phenomena of separation, transition and reattachment, which are intimately linked with the management of the near-wall physics, of the laminar to turbulence transition and of the physical dependence of such phenomena on the values of free-stream turbulence, the main prospects for the developed dynamic procedure. Simulations are performed by varying the grid resolution and the free-stream turbulence levels by keeping a fixed Reynolds number, $Re = U_0 D / \nu = 3333$ where U_0 is the free-stream velocity, D the plate thickness and ν the kinematic viscosity.

4.1. Numerical configuration

Simulations of the new modeling approach are performed by using the solver T-Flows (<https://github.com/DeNov/T-Flows>) (Hadžiabdić *et al.* 2022). T-Flows is based on a finite volume method for collocated, unstructured and arbitrary grids. The transport scheme for momentum and turbulent quantities is SMART, a high-order upwind-biased scheme which maximizes accuracy within the limits required to preserve boundedness (Gaskell & Lau 1988). Time integration is performed with the backward Euler scheme in first-order form for the stresses and in a second-order variant, used in iterative fashion, for the inertial term. The time step is adapted to obtain a condition $CFL \approx 1.5$.

By taking advantage of the statistical symmetries of the mean flow solution, only the top half of the flow domain is solved in line with common industrial approaches based on RANS. A fixed velocity is applied at the inlet while a free-slip condition at the top and at the symmetry plane. A standard Neumann boundary condition is applied at the outlet in order to avoid the potential stability issues related to having a convective outlet adjacent to the finely resolved non-slip wall of the solid body. Finally, periodic boundary conditions are applied in the spanwise direction. The domain extends for $-17 \leq x/D \leq 28$, $0 \leq y/D \leq 17$ and $0 \leq z/D \leq 2$ where (x, y, z) denote the streamwise, vertical and spanwise directions and the reference frame system is centered at the leading edge of the plate. Accordingly, (u, v, w) will hereafter denote the streamwise, vertical and spanwise components of the velocity vector.

The geometric characteristics of the rounded leading edge flat plate offer the possibility of having a structured layout for the grid by adopting a C-type inlet. Two different grids are considered in order to address the sensitivity of the flow solution to spatial discretization, see figure 1. Both grids have a first layer of cells around the plate whose thickness is on average smaller than one friction length. The T3L case exhibits a laminar separation around the end of the circular leading edge and a reattachment at streamwise positions varying with the turbulent intensity of the free stream. Accordingly,

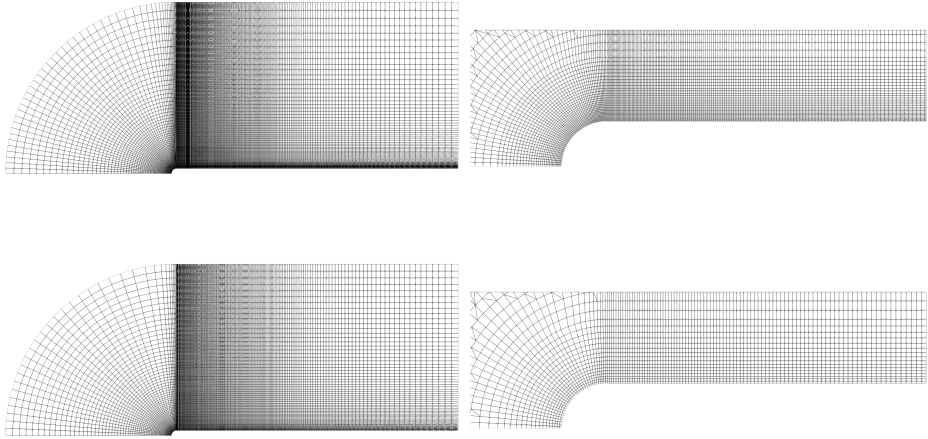


FIGURE 1. Finer (above) and coarser (below) grids for the T3L study. On the left, an overall view of the computational domain is reported while, on the right, a detailed view for $-1 \leq x/D \leq 4$ and $0 \leq y/D \leq 1.5$ is reported to better illustrate the grid resolution.

both grids exhibit a stretching leading to finer spatial resolutions by moving towards the plate in the vertical direction and towards the leading edge in the streamwise direction. The total number of computational elements in the finer grid is 1.03M while for the coarser grid spatial resolution is roughly halved in all 3 directions, resulting in 0.34M numerical volumes. Overall, the spatial resolution adopted for the finer grid evaluated in a refinement box extending for $0.5 \leq x/D \leq 1.2$ and $0.5 \leq y/D \leq 9.3$, is $\Delta x/D = 0.012 \div 0.1$, $\Delta y/D = 0.01 \div 0.046$ and $\Delta z/D = 0.05$ while for the coarser grid is $\Delta x/D = 0.023 \div 0.11$, $\Delta y/D = 0.023 \div 0.073$ and $\Delta z/D = 0.1$. In the present work, we also perform 2D steady-state simulations. For these simulations, the grid employed has the same $x - y$ distribution of the finer 3D grid and counts 25700 computational elements.

4.2. Dynamic procedure settings

4.2.1. Baseline closure

The dynamic RANS procedure developed in section §3.1 represents a new class of turbulence closures, as the procedure can be adapted to any type of two-equation turbulent viscosity closures. In this first attempt, we assess its performance by using the standard $k - \epsilon$ model as baseline closure, in line with the theoretical development reported in section §3.1. A complete assessment of its performance including the effect of a change of the baseline closure is left to future more technical works.

It is important to highlight that standard implementations of the $k - \epsilon$ model make use of a damping function f_μ to limit the value and improve the scaling of eddy viscosity in the near-wall region. This correction to the standard $k - \epsilon$ approach is no longer necessary when adopting the developed dynamic procedure. Indeed, we performed tests with and without damping function f_μ and we found that the dynamic procedure automatically adjusts the eddy viscosity values to the different flow regions thus producing more physically accurate results without the use of artificial corrections to the eddy viscosity field. Accordingly, all the simulations reported in the present work are performed by

using the standard $k - \epsilon$ model as baseline closure without damping functions for the eddy viscosity.

4.2.2. Filter kernels and widths

Apart from the baseline closure, the new dynamic RANS approach presents another important degree of freedom that can lead to different type of implementations: the kernel of the second test filter and its width T . Given the dual nature of the dynamic RANS procedure that ranges from statistical to scale-resolving approaches, the selection of the filter kernel is not straightforward and is addressed here for both approaches separately.

When seeking for a scale-resolving unsteady solution, the simplest choice for the test filter kernel is that given by a backward moving average,

$$\langle \beta \rangle_T(N, t) = \frac{1}{N \Delta t} \int_{t-N \Delta t}^t \beta(t') dt' \quad (4.1)$$

where N is the number of time steps used for computing the moving average and, hence, $T = N \Delta t$. In the present work, we report results of the dynamic procedure for $N = 2$. However, it is worth pointing out that different extensions for the moving average ($N = 3, 5$ and 10) have been evaluated to test the robustness of the proposed dynamic procedure. We found that such alternative implementations produce solutions that do not differ significantly from those reported in the following for $N = 2$.

When seeking for a statistical solution, the definition of the test filter operator is less straightforward. Indeed, the common CFD practice for computing a statistical solution is to use steady-state solvers in order to save computational costs. Steady-state solvers commonly adopt iterative methods that are seeking for a convergence of the flow solution. This convergence is usually achieved by RANS closures due to the high intensity of the modeled stresses introduced into the solution that allows to rapidly reach a statistical solution provided that the separation of scales of the problem is not too large. On the contrary, when the problem under consideration is characterized by a large separation of scales, the intensity of the modeled stresses of RANS closures is not high enough to reach a statistical solution and the iterative solutions of the solver are found to fluctuate. This last scenario is what characterize the dynamic RANS solution when computed using steady-state solvers. Indeed, we have that the modulation of the modeled stresses given by the dynamic procedure leads to variable iterative solutions also in flow problems characterized by a small separation of scales. Because in steady-state solvers the iterative solutions are in general not correlated being not separated by a physical time, a possible choice for the test filter kernel is to use a cumulative algebraic average of the iterative solutions. For a generic quantity β , the resulting test filter operator reads

$$\langle \beta \rangle_T(it_0, it_n) = \frac{1}{it_n - it_0} \sum_{it_0}^{it_n} \beta(it) \quad (4.2)$$

where it_0 is the first iteration used for the algebraic average accumulation and it_n is the last one. In the present work, we start the dynamic RANS steady-state simulations from an initial iterative solution it_0 obtained by running the baseline closure without dynamic procedure.

4.2.3. Clipping procedure

It is worth noting that the dynamic procedure (3.11) can yield negative values for the model coefficient c_μ and, hence, of eddy viscosity with obvious repercussions for the numerical stability of the solution. For this reason, we adopt a clipping procedure that

limits the dynamic coefficient's value to the range $0 \leq c_\mu \leq 0.2$. Extensive tests have again been performed in order to assess the sensitivity of the solution to the imposed upper bound value of c_μ . A small sensitivity of the solution to this value has again been found thus further supporting the robustness of the developed dynamic procedure.

4.3. Free-stream turbulence

Transition, separation and reattachment are key physical features of the T3L case and many other applications and are known to significantly depend on the free-stream turbulence conditions. The common practice of real-world CFD applications, is to prescribe the free-stream turbulence conditions with the inlet boundary conditions of the modeled turbulent kinetic energy and dissipation, k_{in} and ε_{in} . The target of the present work is to improve the CFD practice, that is why we adopt the same approach here. However, this choice makes the prescription of the free-stream turbulence conditions rather complex. Indeed, the inlet boundary conditions experience a decay before impinging to the body that, without loss of generality, can be for example modeled as

$$\left. \begin{aligned} k(x) &= k_{in} \left[1 + \left(C_{\varepsilon 2} - 1 \right) \frac{\varepsilon_{in}}{k_{in}} \frac{x}{U_0} \right]^{-\frac{1}{C_{\varepsilon 2}-1}} \\ \varepsilon(x) &= \frac{k(x) \varepsilon_{in}}{k_{in} \left(1 + \frac{\varepsilon_{in}}{k_{in}} \frac{x}{U_0} \right)} \end{aligned} \right\} \quad (4.3)$$

However, depending on the numerical resolution, numerical schemes and turbulence closure, the actual decay changes. Hence, the inlet boundary conditions must be tuned but it is not always possible to impose the desired free-stream conditions actually perceived by the body. The latter are here evaluated by computing the free-stream turbulence intensity and the free-stream turbulence integral length in a plane $x = -D$,

$$\left. \begin{aligned} I &= \frac{\sqrt{2r k/3}}{U_0} \\ \lambda &= \frac{(r k)^{3/2}}{\varepsilon} \end{aligned} \right\} \quad (4.4)$$

Here, $r = (c_\mu/c_\mu^*)^{1/2}$ is a scaling factor deemed essential to take into account the fact that in the dynamic RANS procedure here developed, the actual free-stream turbulence acting in the momentum equations is modulated by the value of the model coefficient c_μ , contrary to more classical approaches where the model coefficient c_μ^* is prescribed as a constant.

5. Scale-resolving approach: 3D unsteady simulations

We start the assessment of the developed dynamic RANS procedure by considering its performance when scale-resolving simulation settings are adopted. The specific settings of the dynamic procedure have been already reported in section §4.2 but we remind here that for scale-resolving simulations we adopt the backward moving average (4.1) as test filter operator. To have a direct indication of the effect of the dynamic procedure on the solution, results will be compared with those obtained with the baseline model, the standard $k-\varepsilon$ approach with $c_\mu^* = 0.09$. To address the scale-resolving capabilities of the dynamic procedure, results will also be compared with a hybrid LES/RANS approach (Fröhlich & Von Terzi 2008; Spalart 2021). The hybrid closure used in the present work employs the Smagorinsky model in the free-flow regions and relies on the $k-\varepsilon-\zeta-f$ model

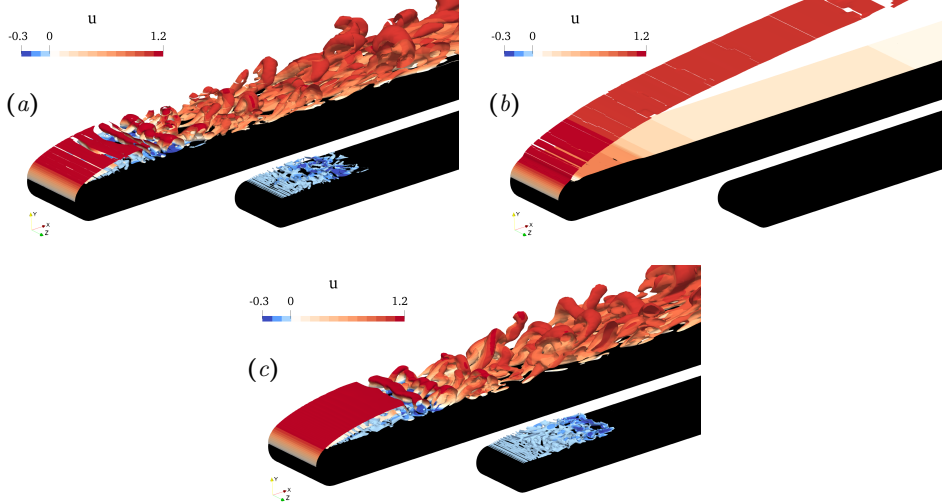


FIGURE 2. Fine-grid scale-resolving simulations of the transitional flow over a rounded leading-edge flat plate. Iso-surfaces of the Q-criterion (Hunt *et al.* 1988), $Q = 0.15$, colored with the streamwise velocity for (a) the new dynamic RANS closure with $I = 0.35\%$, (b) the standard $k - \epsilon$ model with $I = 2.3\%$ and (c) the hybrid LES/RANS model with $I = 0\%$. In the inset plots, iso-surfaces with positive streamwise velocity are hidden to reveal the structures of the reverse boundary layer within the main recirculating bubble.

in the near-wall regions (Hanjalić *et al.* 2004). For further details about the hybrid LES/RANS model, the reader is referred to Delibra *et al.* (2010). Finally, data from high-fidelity implicit-LES simulations performed by Bassi *et al.* (2020) will be considered as a reference.

Different free-stream turbulence conditions are simulated by varying the free-stream boundary conditions of the modeled turbulent kinetic energy and dissipation, k_{in} and ε_{in} respectively. By following the procedure reported in section §4.3, the imposed values of k_{in} and ε_{in} are designed in order to systematically change the turbulence intensity I perceived by the body while keeping the integral length almost constant $\lambda = D/2$. Statistics are computed by performing a spatial average in the spanwise direction and a temporal average based on 60 flow samples gathered every $6L/U_0$ times after reaching a fully developed flow solution. The resulting average operator is hereafter denoted as $\langle \cdot \rangle$.

5.1. Instantaneous flow pattern

The instantaneous flow pattern taken by the new dynamic RANS approach is reported in figure 2(a). A fully unsteady and 3D flow pattern is reproduced. First, an almost laminar shear layer is developed that takes origin from the separation of the boundary layer around the beginning of the flat portion of the plate. The shear layer is then found to develop Kelvin-Helmholtz instabilities taking the form of spanwise vortex tubes spanning the entire domain width. By moving downstream, the spanwise vortices undergo a further instability in the form of a lift up and stretching thus forming hairpin-like structures arranged in a staggered manner (Cimarelli *et al.* 2018). After reattachment, these hairpin-like structures are further stretched by mean shear thus developing streamwise vortices which are known to induce high- and low-speed streaks that dominate the downstream development of the attached boundary layer. To note that within the recirculating bubble,

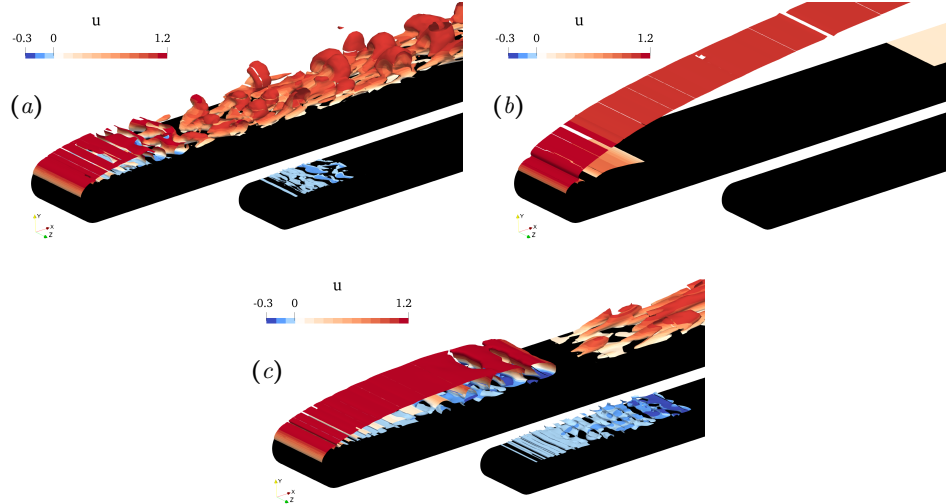


FIGURE 3. Coarse-grid scale-resolving simulations of the transitional flow over a rounded leading-edge flat plate. Iso-surfaces of the Q-criterion (Hunt *et al.* 1988), $Q = 0.15$, colored with the streamwise velocity for (a) the new dynamic RANS closure with $I = 0.5\%$, (b) the standard $k - \epsilon$ model with $I = 2.5\%$ and (c) the hybrid LES/RANS model with $I = 0\%$. In the inset plots, iso-surfaces with positive streamwise velocity are hidden to reveal the structures of the reverse boundary layer within the main recirculating bubble.

a reverse boundary layer also takes place that as highlighted in the inset of figure 2(a) is also fully turbulent.

As shown in 2(b), the baseline $k - \epsilon$ model completely misses all the degrees of freedom of the solution. Indeed, a stationary 2D solution is reproduced that lacks the turbulent structure that would otherwise be supported by the grid resolution, as demonstrated by the dynamic RANS closure. Such a scale-resolving feature of the dynamic RANS procedure is indeed recovered when considering scale-resolving methods such as the hybrid LES/RANS approach reported in 2(c). In conclusion, the spatial resolution adopted supports a large number of degrees of freedom in the solution that are unlocked by the new dynamic RANS approach and by the hybrid LES/RANS model, and which would otherwise be missed by using standard statistical closures such as the $k - \epsilon$ model.

As shown in figure 3(a), by coarsening the spatial resolution, the flow solution of the dynamic RANS model still reproduces the relevant flow structures highlighted so far for the finer grid. The only difference is simply given by the fact that the smaller flow structures reproduced by the finer grid are not anymore captured for obvious reasons of spatial resolution. Such a robustness of the dynamic RANS approach to the coarsening of the resolution is not observed for the hybrid LES/RANS approach. Indeed, as shown in figure 3(c), the flow solution of the hybrid LES/RANS method suffers a strong deterioration of the resolved flow physics that is not limited to the sole absence of fine scale structures in the flow solution. It consists also in a strong degradation of relevant flow features such as the large-scale dynamics of the recirculating bubble whose length scale is widely overestimated and whose structure is reduced to almost two-dimensional spanwise rolls.

The robustness of the dynamic RANS closure to the coarsening of the spatial resolution is a remarkable feature rendering it particularly interesting for CFD applications in real-

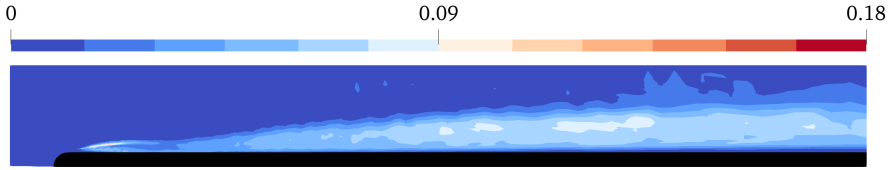


FIGURE 4. Average behaviour of the model coefficient c_μ obtained by the dynamic RANS closure for the scale-resolving 3D unsteady simulations performed in the fine grid.

world problems. This relevant property stems from the fact that the developed model is a RANS closure in nature wherein the dynamic procedure locally adapts to the spatial resolution by enabling scale-resolving features also in ambiguous grids. Indeed, when coarsening the grid resolution, larger portions of the flow domain call for an increase of the modeled stresses that would asymptotically converge to that provided by statistical approaches typical of pure RANS closures. These transitional and fully modeled regions are better captured by the developed dynamic RANS closure thanks to its ability in improving the flow solution also in statistical approaches as it will be demonstrated in section §6 through the analysis of 2D steady simulations.

5.2. Dynamic model coefficient

In order to address the ability of the dynamic RANS closure to automatically adapt to different flow physics and in enabling scale-resolving features, we analyse here the behaviour of the model coefficient c_μ shown in figure 4. In the leading-edge shear layer, the dynamic procedure reproduces its transitional physics. It consists of small values of the model coefficient in the first laminar part and in a gradual downstream increase in its intensity that matches the development of increasingly higher levels of turbulence. As a result the dynamic RANS closure is able to reproduce laminar to turbulence transition. This property of the dynamic RANS closure is of overwhelming relevance for actual CFD applications. As shown in figure 4, the model coefficient is found to be activated by the dynamic procedure also in the reverse boundary layer within the leading-edge recirculating bubble and in the downstream development of the attached boundary layer. Also in this case, the dynamic procedure is found to reproduce the physics of the problem that for boundary layers consists in a strongly inhomogeneous phenomenology of momentum transport that is dominated by viscous diffusion in the near-wall region and by turbulence mixing in the bulk of the flow. In fact, the model coefficient c_μ is found to dynamically adapt to these different physics of the boundary layer. In particular, the model coefficient is found to assume values similar to the ones classical employed in standard $k - \varepsilon$ implementations, $c_\mu = 0.09$, in the bulk of the flow where turbulence mixing dominates momentum transport. From these values, the model coefficient is found to decrease by moving towards the wall thus naturally adapting to the low Reynolds number behaviour of the near-wall region. This property is again of relevance for actual CFD applications. Indeed, as already stated in section §4.2.1, this scaling of c_μ allows to avoid the use of near-wall damping functions whose use is critical especially in separating and reattaching flows typical of the applications. In conclusion, the dynamic RANS closure is able to adapt to the strongly inhomogeneous physics of the different flow regions by activating the dynamic coefficient c_μ in the fully turbulent regions and by suppressing it in the laminar viscosity-dominated ones even in flow regions characterized by high shear rates such as the very near-wall region and the initial laminar stage of the leading-edge shear layer.

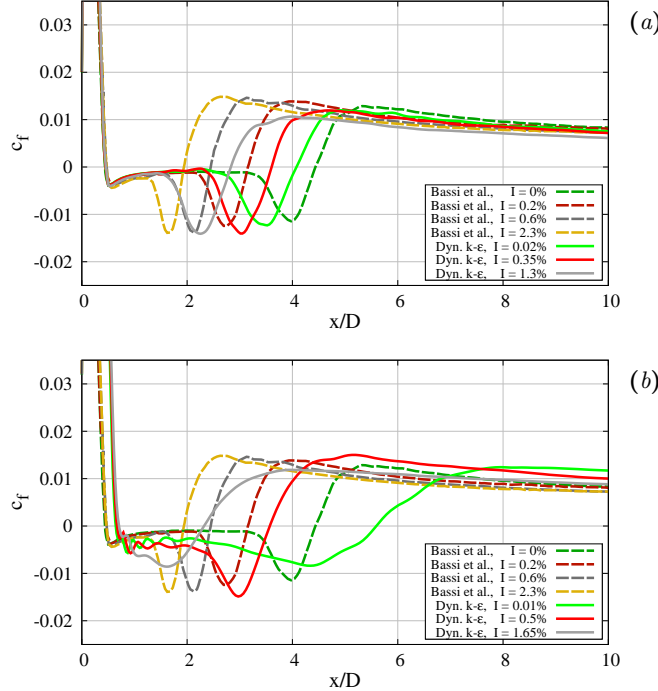


FIGURE 5. Average friction coefficient for the scale-resolving 3D unsteady simulations performed in (a) the fine and (b) coarse grids of the new dynamic RANS closure compared to the high-fidelity implicit-LES simulations performed by Bassi *et al.* (2020).

5.3. Friction coefficient

The ability to deal with laminar flows and predict transition is one of the main prospects for the developed dynamic RANS closure. In this respect, the laminar separation, transition and turbulent reattachment events that characterize the T3L flow case make it very suitable to test the ability of closures in addressing these phenomena. In order to quantitatively assess the capability of the different turbulence closures in accurately capturing such flow features we report the behaviour of the friction coefficient c_f . As shown in figure 5(a), the new dynamic RANS approach is found to reproduce the phenomena of laminar separation, transition and turbulent reattachment and to capture their dependence on the value of free-stream turbulence. In particular, the shape of the friction coefficient profile reproduces that exhibited by the high-fidelity implicit-LES simulations performed by Bassi *et al.* (2020) thus showing that the physics of the phenomena involved in the flow system is nicely captured. Furthermore, the expected shrinking of the separation bubble and reduction of the reattachment length for increasing free-stream turbulence levels is also nicely reproduced thus showing that the dynamic RANS closure allows to capture flow phenomena such as transition that are sensitive to the free-stream turbulence level. When coarsening the resolution, the resolved physics deteriorates as shown in figure 5(b). However, the main features of the flow are still captured, namely the gross shape of the friction coefficient profile and its dependence on the free-stream turbulence.

The degree of improvement of the physics captured by the new modeling approach becomes apparent when comparing the behaviour of the friction coefficient with that obtained by using the baseline $k - \varepsilon$ approach. As shown in figure 6(a), the standard

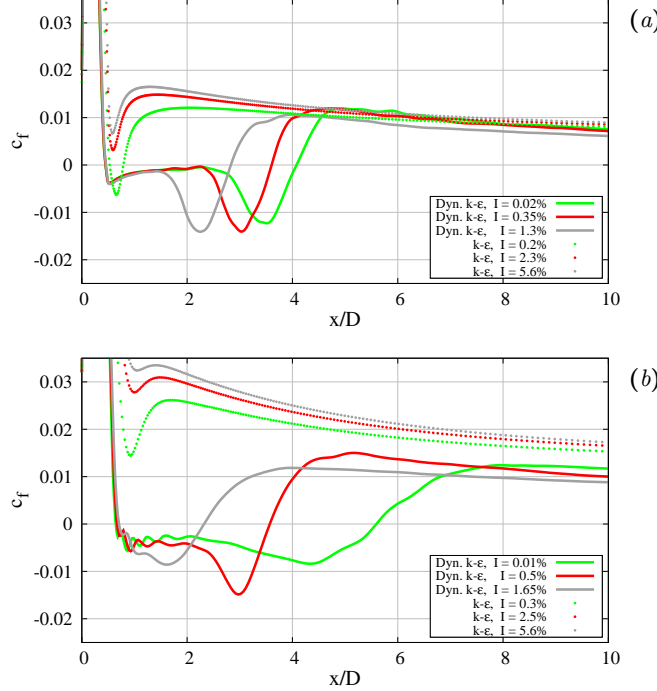


FIGURE 6. Average friction coefficient for the scale-resolving 3D unsteady simulations performed in (a) the fine and (b) coarse grids of the new dynamic RANS closure compared to the standard $k - \varepsilon$ approach.

$k - \varepsilon$ model completely fails in capturing the laminar separation. Actually, the boundary layer developing at the leading edge is always turbulent and, as a consequence, the flow does not separate with except to a very small recirculating bubble for the flow case at the lower free-stream turbulence level. The scenario becomes even worse when coarsening the resolution. As shown in figure 6(b), the physics of the leading-edge boundary layer is so poor that affects the entire downstream development of the flow. Overall, the poor performances of the baseline $k - \varepsilon$ model are related to its well-known tendency to over-predict eddy viscosity in areas of the flow which should be laminar and transitional. As a consequence, the separation of the leading-edge boundary layer is almost always prevented, rendering the $k - \varepsilon$ model unsuitable for transitional separating and reattaching flows. In this context, the adoption of the present dynamic procedure to the $k - \varepsilon$ model makes it possible to solve all these problems.

The developed dynamic procedure has shown to be able to capture relevant unsteady and 3D coherent structures of turbulence and transitional phenomena in separating and reattaching flows. Accordingly, it appears that the dynamic RANS model enables classical eddy viscosity models to capture relevant turbulent or transitional flow features when the grid resolution allows to represent them. This is a typical feature of scale-resolving methods that is why we compare also our results with those of the hybrid LES/RANS model. As shown in figure 7(a), the shape of the friction coefficient profile for the hybrid LES/RANS approach highlights that the physics of laminar separation, transition and turbulent reattachment is reproduced as much as that of the new dynamic RANS closure. The hybrid model is, however, found to be unresponsive to changes in the boundary conditions for k and ε . This lack of sensitivity is caused by the LES-like mode that is

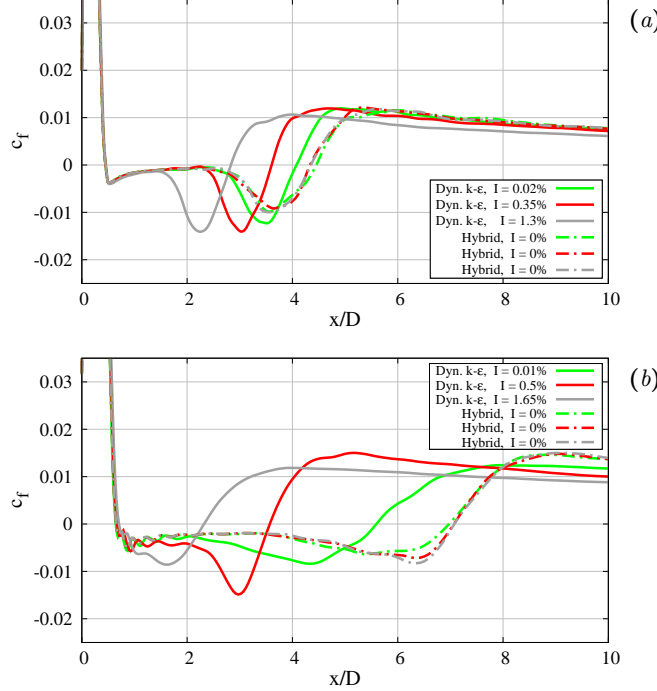


FIGURE 7. Average friction coefficient for the scale-resolving 3D unsteady simulations performed in (a) the fine and (b) coarse grids of the new dynamic RANS closure compared to the hybrid LES/RANS approach.

operated in the region of the domain between the inlet and the solid body. As a result, the free-stream turbulence intensity cannot be imposed through boundary conditions on k and ε , but should instead be generated through a forcing plane and then directly resolved as it is in all scale-resolving methods. In the present simulations such a forcing plane is not implemented and, as a result, the free-stream turbulence intensity that reaches the plate is extremely low (virtually zero) regardless of the imposed inlet boundary conditions. This makes the hybrid LES/RANS approach incapable of correctly modeling the effect of free-stream turbulence intensity through boundary conditions contrary to the present dynamic RANS approach. This is a key aspect that makes the present dynamic RANS procedure definitely favorable for the numerical solution of complex flows commonly encountered in applications.

Finally, let us point out that when coarsening the spatial resolution, the resolved physics deteriorates more for the hybrid LES/RANS approach than for the present dynamic RANS model, see figure 7(b). As already pointed out when analysing the instantaneous flow pattern reported in figure 3, the quality of the solution increasingly relies on the ability of the closure in capturing the physics of the regions calling for a modeled stress increase as they become larger when coarsening the resolution. The developed dynamic RANS approach is found to outperform in transitional regions where scale-resolving features are partially supported by the grid and in the fully modeled regions by improving the flow solution with respect to classical pure RANS closures as it will be demonstrated in §6 through the analysis of 2D steady simulations. This is a fundamental feature rendering the present dynamic formulation more suitable for real-

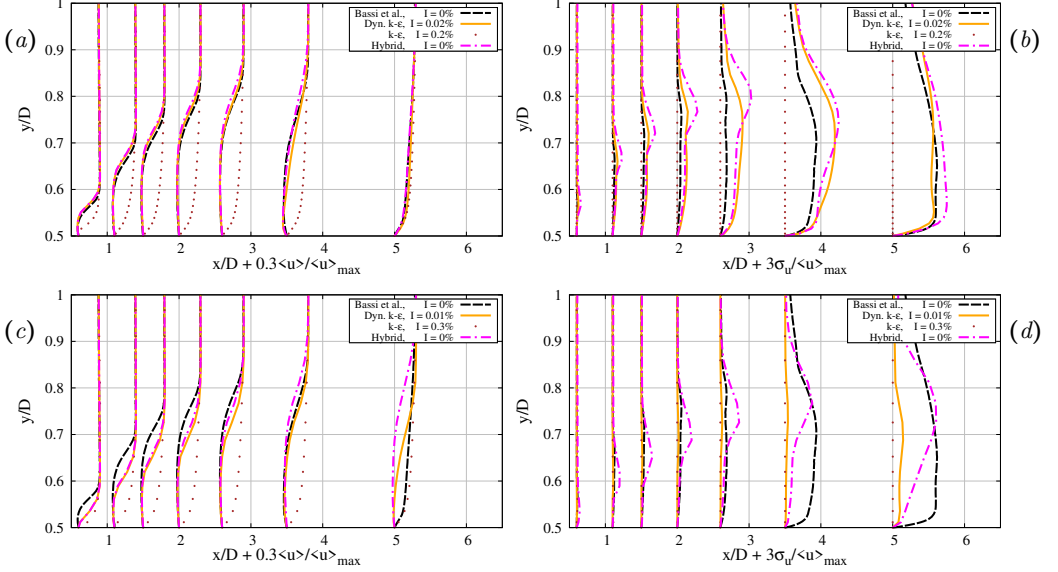


FIGURE 8. Mean streamwise velocity profiles (a) and (c) and mean streamwise turbulent intensities (b) and (d) at the lowest free-stream turbulence level. Results from scale-resolving simulations performed on the fine grid (a) and (b) and on the coarse grid (c) and (d). The dynamic RANS formalism, the $k - \varepsilon$ model and the hybrid LES/RANS approach are compared with the high-fidelity implicit-LES simulations performed by Bassi *et al.* (2020).

world CFD applications where the grid resolution assigns the task of solving the flow to statistical closures in large portions of the domain.

5.4. Mean velocity and turbulent profiles

To further assess the quality of the transitional flow solutions over a rounded leading-edge flat plate achieved by the different modeling approaches, we address here the wall-normal profiles of the mean streamwise velocity $\langle u \rangle$ and of the standard deviation of streamwise velocity $\sigma_u = \sqrt{\langle u' u' \rangle}$ at different streamwise locations. As shown in figure 8(a) and (b), the dynamic RANS and hybrid LES/RANS closures show a similar behaviour on the finer grid, well reproducing the scaling of the mean velocity and turbulent profiles of the reference implicit-LES simulation (Bassi *et al.* 2020). The main discrepancy is an overestimation of the intensity of turbulent fluctuations along the leading-edge shear layer developing in the initial part of the separating bubble. However, the overall phenomena of laminar separation, transition and turbulent reattachment are found to be nicely captured by the two modeling approaches in accordance with the analysis of the previous sections. On the contrary, the baseline $k - \varepsilon$ model completely fails in reproducing the flow separation thus confirming again its inadequacy in capturing laminar boundary layer separation.

When coarsening the grid resolution, the accuracy of the flow phenomena deteriorates as shown in figure 8(c) and (d). In particular, a significantly longer flow recirculation is reproduced by both the dynamic RANS and hybrid LES/RANS closures as already shown when analysing the friction coefficient in figure 7(b). As a consequence, the mean standard deviation profiles of streamwise velocity are significantly misaligned with respect to those of the reference implicit-LES solution. In any case, the solution exhibits a slightly better behavior for the dynamic RANS approach than for the hybrid LES/RANS approach.

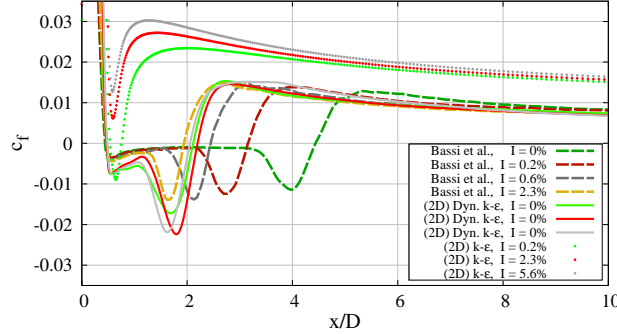


FIGURE 9. Average friction coefficient for the statistical 2D steady simulations performed with the new dynamic RANS formalism and with the standard $k - \epsilon$ model. Results are compared with the high-fidelity implicit-LES simulations performed by Bassi *et al.* (2020).

The solution of the baseline $k - \epsilon$ model is found to be less sensitive to the coarsening of the mesh but still completely failing in reproducing the flow physics.

6. Statistical approach: 2D steady simulations

One of the distinctive features of the proposed dynamic formalism is its ability to automatically switch from scale-resolving to statistical approaches depending on the numerical setup employed. This is a key property for applications where the latter are still widely used. In order to explore the potential of the proposed dynamic RANS closure also in statistical approaches, we report here results of the T3L flow case simulated in steady-state and 2D conditions. This setup is not suitable for scale-resolving methods such as the hybrid LES/RANS approach that is why results of the proposed dynamic RANS approach will be compared solely with those of the baseline $k - \epsilon$ model together with the high-fidelity implicit-LES simulations performed by Bassi *et al.* (2020) as a reference. Statistics are obtained by averaging among the last 900 iterations of the simulations. The specific settings of the dynamic procedure have been already reported in section §4.2 but we remind here that for steady-state simulations we adopt an accumulation between successive iterations (4.2) as test filter operator.

The behaviour of the friction coefficient c_f is reported in figure 9. The friction coefficient profiles resulting from the 2D dynamic RANS simulations reveal substantial differences with respect to those obtained through 3D simulations. They consist in a overestimation of the negative peak of c_f within the reverse boundary layer and in the loss of responsiveness to the inlet boundary conditions meant to model the free-stream turbulence intensity. The latter is essentially induced by the fact that the dynamic procedure sets the model coefficient c_μ to extremely small values in the upstream flow region. Hence, the free-stream turbulence level perceived by the body is always virtually zero, regardless of the free-stream conditions imposed through the inlet boundary conditions of k and ϵ . Despite these deficiencies, the dynamic RANS simulations still yield a distinct reproduction of the main features of the flow and a correct evaluation of the intensity of the c_f along the downstream development of the attached boundary layer. The quality of these features becomes apparent when comparing these results to those obtained with the baseline $k - \epsilon$ model. Indeed, the $k - \epsilon$ model does not capture

transition thus drastically reducing or preventing separation. The friction coefficient is then largely overestimated thus affecting the entire downstream development of the flow. In particular, the values of the friction coefficient are found to remain overestimated also along the downstream evolution of the attached boundary layer. Overall, these results show that the developed dynamic formalism leads to a significant improvement of the quality of the solution also in statistical approaches. This is a fundamental property for most of CFD applications and explains the improved performances that the dynamic RANS closure exhibits also in scale-resolving approaches when coarsening the grid, as already observed in section §5.

7. Conclusions

It is well known that numerical solutions of the equations of motion adopting statistical turbulence closures predict unsteady flow patterns in certain flow problems where the average solution is on the contrary steady. It is also well known that the combination of statistical and scale-resolving closures, the so-called hybrid approaches, allows to capture the turbulent structure of the solution in many flow problems. The numerical approaches provided by both statistical and hybrid closures are widely used in CFD applications but lack a clear theoretical framework for their assessment and improvement. From one side, the formalism provided by the exact RANS equations that is based on the average operator does not predict unsteady nor scale-resolving flow solutions. From the other side, the formalism provided by the exact LES equations that is based on a spatial filtering operator does not predict the loss of scale-resolving features in the flow solution. These simple facts suggest that an alternative theoretical framework must be used to assess and eventually develop turbulence closures when employed in very-coarse steady and unsteady numerical settings typical of CFD applications.

7.1. A change of paradigm: temporally filtered Navier-Stokes equations

In the present work we propose an alternative operatorial approach for the development of an exact theoretical framework that is able to describe the smoothing action of turbulence closures in both statistical and scale-resolving approaches. The basic assumption is that such a smoothing action can be described by a temporal filtering operator. As a consequence, the proper exact theoretical framework for turbulence closures ranging from the statistical to the scale-resolving ones, is represented by the temporally filtered Navier-Stokes equations. Indeed, the relevant aspect of this exact formalism is given by the fact that the related turbulent stresses $R(u_i, u_j) = \langle u_i u_j \rangle_\tau - \langle u_i \rangle_\tau \langle u_j \rangle_\tau$ smoothly converge from those related to scale-resolving methods (subgrid stresses) to those related to statistical approaches (Reynolds stresses) by increasing the filter time scale τ . In other words, the temporally filtered Navier-Stokes equations represent an unifying exact theoretical framework that provide a direct link between the scale-resolving and statistical approaches. In particular, scale-resolving approaches are interpreted as the result of a turbulence closure whose additional stresses are associated to a filter time scale that is not large enough to recover the averaged solution, i.e. $\tau U/L \leq 1$ and $\langle \cdot \rangle_\tau \neq \langle \cdot \rangle$. On the other hand, statistical approaches are interpreted as the result of a turbulence closure whose additional stresses are associated to a very large filter time scale, i.e. $\tau U/L \gg 1$ and $\langle \cdot \rangle_\tau = \langle \cdot \rangle$. The temporally filtered Navier-Stokes equations and their link between the statistical and scale-resolving approaches have already attracted some interest in scientific community (Pruett *et al.* 2003; Pruett 2008; Fadai-Ghotbi *et al.* 2010; Friess *et al.* 2015; Duffal *et al.* 2022). The potential of this framework is highlighted here by

unveiling its relevant fundamental properties and by deriving a new class of turbulence closures able to bridge between scale-resolving and statistical approaches.

7.2. Dynamic RANS closures

Beyond providing an exact theoretical framework for actual CFD implementations, the proposed change of paradigm enables a very important algebraic property that can be leveraged to improve the predictive capabilities of RANS eddy viscosity models. It consists in a exact relation between turbulent stresses at different temporal filter levels that we use to develop a dynamic procedure for the calculation of the model coefficient c_μ appearing in the definition of eddy viscosity that for a standard $k - \varepsilon$ approach reads $\nu_\tau = c_\mu k_\tau^2 / \epsilon_\tau$. The results highlight that the developed dynamic RANS closure shows accurate scale-resolving properties when the numerical settings and the grid resolution allow them to develop. In particular, the dynamic RANS model is found to capture challenging flow features such as the laminar to turbulence transition and the dependency of the boundary layer separation and reattachment to changes in the free-stream turbulence applied as boundary condition. These are two key properties of overwhelming relevance for CFD applications where separating and reattaching phenomena are often present whose features are heavily dependent on transition and free-stream turbulence. The dynamic RANS formalism is found to outperforms also when the grid resolution is coarsened. The reason is the improved physics captured by the dynamic RANS closure also when employed in statistical approaches. Indeed, the regions of the flow that call for a modeled stress increase typical of statistical approaches, widen with the coarsening the grid. As a consequence, the quality of the entire flow solution increasingly relies on the quality of the solution in the fully modeled regions. Tests of the dynamic RANS closure when employed as a statistical closure in 2D steady-state numerical settings, reveal a significant improvement of the flow physics captured especially in the laminar to turbulence transitional regions where the tendency of the baseline $k - \varepsilon$ approach to over-predict eddy viscosity is avoided. As a result, the dynamic RANS formalism is found to be robust to a coarsening of the spatial resolution in scale-resolving approaches.

7.3. Perspectives

Overall, the improved performances in scale-resolving unsteady approaches (in terms of ability of capturing laminar to turbulence transition, of responsiveness to the free-stream turbulence levels applied through the boundary conditions and of robustness to a coarsening of the spatial resolution) and the improvement of the physics of the solution captured in statistical steady-state approaches, render the developed dynamic RANS closure promising for actual CFD applications. This result sets the stage for further more technical studies that are deemed essential to identify the best implementation of the model and to address its performance with respect to a wider range of closures. As a matter of facts, the developed dynamic RANS closure actually represents a general formalism that forms a class of turbulence closures where the dynamic procedure can be applied to different eddy viscosity models. Hence, the present implementation based on the standard $k - \varepsilon$ closure is just one version over many possible and can be reasonably improved by adopting more advanced closures, e.g. $k - \omega$ and $k - \omega$ SST. Hence, further studies addressing the best implementation of the dynamic RANS procedure and its performance with respect to a variety of scale-resolving and statistical closures are envisaged and left to future more technical works.

7.4. Technical remarks

Apart from being a unifying formalism for scale-resolving and statistical approaches, the temporally filtered Navier-Stokes equations exhibit two relevant properties that are remarked here. First, it is more easy to make the temporal filtering operator commutative with respect to differential operators. Indeed, this commutative property can be easily achieved by actual numerical implementations by adopting a constant time step. This property is generally missed by actual implementations of the spatially filtered Navier-Stokes equations such as those employed in LES, because the spatial resolution needs to be almost always adapted to the physics of the different flow regions thus making the spatial filtering operator non-commutative with the spatial derivatives (Klein & Germano 2020). The second relevant property of the temporally filtered Navier-Stokes equations is related to the use of explicit filtering operator such as those employed here in the dynamic RANS approach. Indeed, an explicit filter kernel can be applied to all the flow regions without ambiguity in the temporal filtering formalism, contrary to the spatially filtered one typical of LES where the definition of its kernel is challenging because of issues related to boundary constraints imposed by the problem geometry and to the stretching of the grid.

Finally, let us remark a basic aspect of the dynamic RANS closure here developed. The model definition does not explicitly involves the temporal and spatial resolution employed for the numerical solution of the equations of motion. Such information is usually explicitly taken into account in scale-resolving approaches, the most famous example is the Smagorinsky model for LES where the grid resolution is explicitly used to define the value of the eddy viscosity. On the contrary, such information is not explicitly included in statistical closures because their solution is independent on the numerical resolution by definition, the most famous example are the two-equation eddy viscosity models for RANS. The present dynamic RANS closure is developed to span scale-resolving and full statistical approaches. Hence, an explicit dependence on the numerical resolution on the model definition is not adopted on purpose in order to address also statistical approaches. On the other hand, the dependence on the spatial and temporal resolution is implicitly recovered by the dynamic procedure itself when addressing problems with a scale-resolving approach. In particular, the dynamic RANS procedure is based on a measure of the change of the solution among two time scales through the use of the test filter (4.1). The spatial resolution determines the type of turbulence structures that can be generated and that span these two time scales. Eventually, the dynamic procedure adapts the eddy viscosity through equation (3.11) to not dissipate them. In other words, the spatial and temporal filtering implicitly performed by the dynamic eddy viscosity when employed in scale-resolving approaches is strictly dependent on the numerical resolution adopted although not explicitly taken into account in the model definition.

Acknowledgements

We wish to acknowledge professors Antonella Abbá and Massimo Germano for the fruitful discussions on the preliminary draft of the present work.

Declaration of Interests

The authors report no conflict of interest.

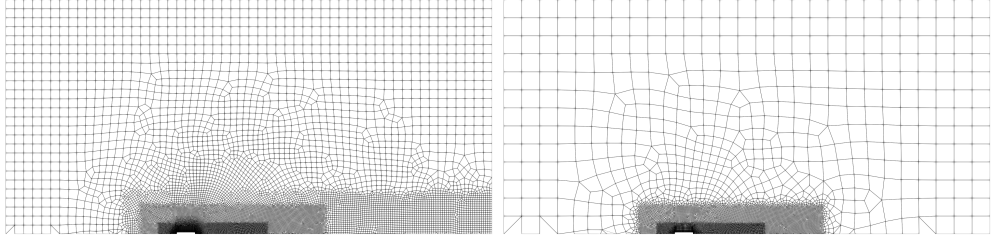


FIGURE 10. Fine (left) and coarse (right) grids developed for the simulation of the flow around a rectangular cylinder with aspect ratio 5.

Appendix A. Flow solutions around a rectangular cylinder

To further assess the performances of the developed dynamic RANS approach, the flow around a rectangular cylinder with aspect ratio 5 is also simulated. This flow case is the object of an international initiative known as BARC (Benchmark on the Aerodynamics of a Rectangular 5:1 Cylinder) (Bruno *et al.* 2014) and several numerical studies have been conducted, see e.g (Mannini *et al.* 2010; Wornom *et al.* 2011; Cimarelli *et al.* 2018; Chiarini & Quadrio 2021; Crivellini *et al.* 2022). Among others, a Direct Numerical Simulation (DNS) at a fairly high Reynolds number $Re = U_0 D / \nu = 14000$ has been recently reported by Cimarelli *et al.* (2024). Here, U_0 is the free-stream velocity and D is the thickness of the rectangular cylinder. The distinguishing feature of the BARC case compared to the T3L case, is the laminar boundary layer separation that is fixed at the sharp leading-edges of the body.

The numerical schemes and the dynamic procedure settings are those used for the simulations of the T3L case and reported in sections §4.1 and §4.2. A constant time step is adopted in order to obtain a condition $CFL \approx 1.5$. In order to study the effect of the grid resolution, two grids have been developed. Both grids are stretched in order to increase the spatial resolution by moving towards the plate in the y -direction and towards the leading- and trailing-edges in the x -direction. The finer grid is composed by $2.48M$ mesh elements and is shown in figure 10. The resulting spatial resolution evaluated in a refined box surrounding the rectangular cylinder up to a distance $1.5D$, is $\Delta x/D = 0.027 \div 0.05$, $\Delta y/D = 0.0028 \div 0.068$ and $\Delta z/D = 0.1$. On the other hand, the coarser grid has been obtained by roughly halving the number of cells in the spanwise z -direction and in the $(x - y)$ -plane, thus leading to a total number of $0.92M$ grid elements, see again figure 10. The resulting spatial resolution evaluated again in a box surrounding the rectangular cylinder up to a distance $1.5D$, is $\Delta x/D = 0.023 \div 0.15$, $\Delta y/D = 0.0028 \div 0.11$ and $\Delta z/D = 0.14$. A free-stream velocity U_0 is imposed at the inlet and at the top and bottom boundaries. A convective boundary condition is applied at the outlet and periodic boundary conditions are imposed in the spanwise direction. Finally, statistics are computed by averaging in the spanwise direction and over 140 time samples collected every $5D/U_0$ times once the flow has reached a fully developed state. The resulting average operator is hereafter denoted as $\langle \cdot \rangle$.

The instantaneous flow solutions are reported in figure 11. Analogously to the T3L flow case analysed in the main body of the present work, the solution obtained with the dynamic RANS procedure is found to capture 3D and unsteady flow structures typical of the flow around rectangular cylinders (Cimarelli *et al.* 2018), see figure 11(a). Furthermore, the dynamic RANS solution is also capable of spawning and transporting turbulent structures in the reverse boundary layer within the main recirculating bubble.

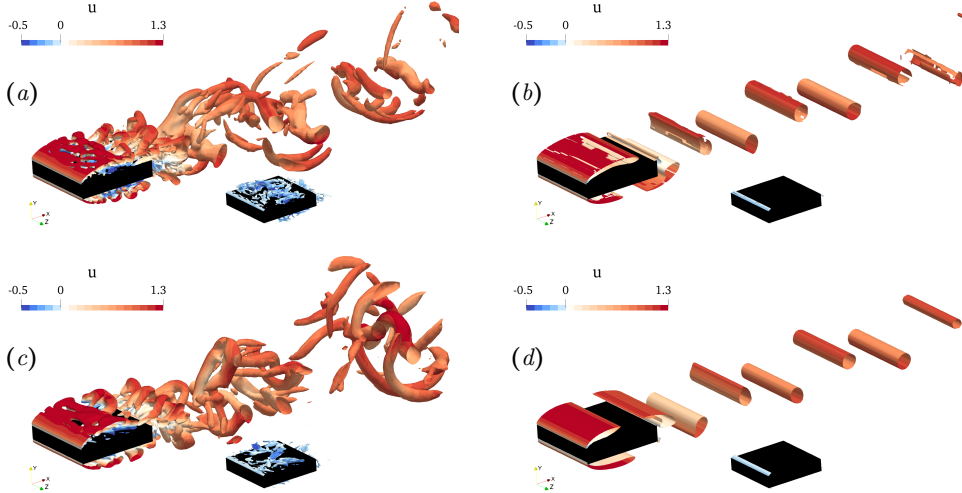


FIGURE 11. Separating and reattaching flow around a rectangular cylinder. Instantaneous flow realizations reported with iso-surfaces the Q-Criterion (Hunt *et al.* 1988), $Q = 0.15$, colored with streamwise velocity. In the inset panels, isosurfaces with positive streamwise velocity are hidden to reveal the structures of the reverse boundary layer within the main recirculating bubble. Flow solutions obtained with the dynamic RANS approach are reported in (a) and (c) for the finer and coarser grids respectively. Flow solutions obtained with the standard $k - \varepsilon$ implementation are reported in (b) and (d) for the finer and coarser grids respectively.

	c_d	σ_{c_l}	St
DNS (Cimarelli <i>et al.</i>)	1.038	0.63	0.111
Dyn. $k - \varepsilon$ (fine)	1.029	0.69	0.116
Dyn. $k - \varepsilon$ (coarse)	1.080	0.92	0.112
$k - \varepsilon$ (fine)	1.064	0.66	0.122
$k - \varepsilon$ (coarse)	1.056	0.54	0.118

TABLE 1. Average drag coefficient c_d , standard deviation of the lift coefficient σ_{c_l} and Strouhal number of the vortex shedding $St = fU_0/D$ measured by using the frequency f of the peak of the lift coefficient spectrum.

When coarsening the spatial resolution, the dynamic RANS solution is found to maintain these flow features thus highlighting a certain degree of robustness of the approach, see figure 11(c). Indeed, the only difference is the obvious lack of fine scale structures in the coarser grid solution. Contrary to the dynamic RANS, the standard $k - \varepsilon$ implementation completely misses the phenomenological features of the separating and reattaching flow by reproducing a flow solution composed by 2D, albeit unsteady, structures, see figures 11(b) and (d).

From a statistical point of view, the quality of the solution is addressed first by evaluating the predictions of the aerodynamic forces, in particular the drag coefficient, the standard deviation of the lift coefficient and the Strouhal number of vortex shedding. As shown in table 1, the dynamic RANS formalism nicely reproduces such quantities when compared with DNS data from Cimarelli *et al.* (2024) with a slight deterioration of the estimates with the coarsening of the grid. Despite the poorly reproduced physics, these integral quantities are also well reproduced by the standard $k - \varepsilon$ model.

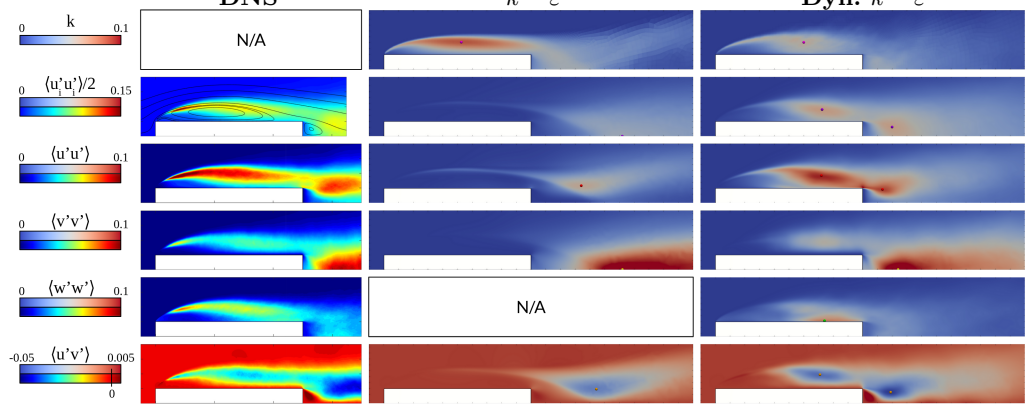


FIGURE 12. Turbulent kinetic energy and Reynolds stresses in the flow around a rectangular cylinder. The left panels report the behaviour obtained from DNS (Cimarelli *et al.* 2024) while the central and right panels show the solution from the standard $k - \varepsilon$ and dynamic RANS approaches, respectively.

The behaviour of turbulent kinetic energy and of Reynolds stresses for the dynamic RANS and standard $k - \varepsilon$ models is reported in figure 12 compared with results from DNS data (Cimarelli *et al.* 2024). When considering turbulent kinetic energy, both the resolved and modelled contributions are reported, $\langle u'_i u'_i \rangle / 2$ and k respectively. Only the results from the finer grid simulations are reported for brevity and because the results from the coarser grid are not too different. The difference between the dynamic RANS and standard $k - \varepsilon$ solutions is marked. As already pointed out, the standard $k - \varepsilon$ model introduces a high amount of eddy viscosity thus damping all turbulent fluctuations except to a shedding of two-dimensional vortices. As a result, the resolved turbulent kinetic energy is very weak compared to the modelled one. For the same reason, the Reynolds stresses are much lower in intensity with respect to those predicted by the reference DNS. The only exception are the cross-stream fluctuations $\langle v' v' \rangle$ in the near wake as a consequence of the higher intensity associated to the shedding of 2D vortices. On the contrary, the dynamic RANS formalism adjusts the eddy viscosity to be compliant with the spatial resolution available, thus allowing for the proper development of a wide range of turbulent structures. As a matter of facts, the resolved turbulent kinetic energy and Reynolds stresses reproduce those of the reference DNS quite well in both shape and intensity.

Appendix B. Turbulent flow over a bump

As a final assessment of the dynamic RANS formalism, we address here its solution in the turbulent flow over a bump. The flow settings consist in a fully turbulent channel with a bump in the bottom wall that produces a turbulent flow separation. Hence, the main difference with respect to the previous flow settings is the absence of laminar to turbulent transitional phenomena. The specific flow settings are those corresponding to the flow case A3 addressed through DNS by Mollicone *et al.* (2017). It corresponds to a bulk Reynolds number $Re_b = U_b h / \nu = 10000$, where U_b is the bulk velocity and h is the channel half height.

The numerical schemes and the settings of the dynamic RANS procedure are the same used for solving the previous flow configurations. Again, two grids have been generated to address the model's performance by varying the spatial resolution. The finer mesh

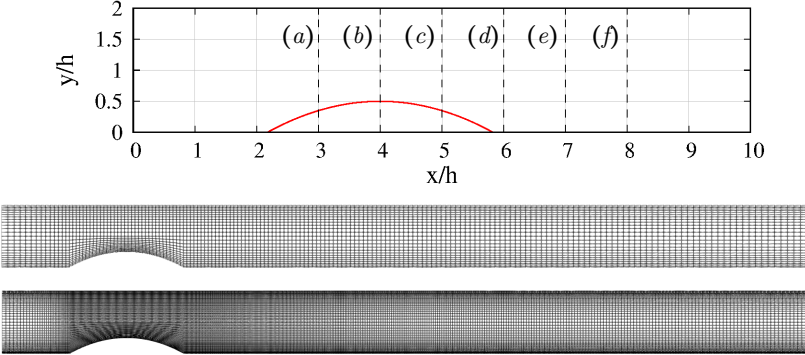


FIGURE 13. Geometry of the bump (top), numerical domain and mesh discretization for the coarse (central) and finer grid (bottom) of the turbulent flow over a bump. The dashed lines in the top panel report the streamwise positions (denoted with letters from *a* to *f*) where the mean and turbulent profiles are evaluated and reported in figures 15 and 16.

is composed of $2.8M$ volumes that are stretched by moving towards the two walls in the wall-normal y -direction and by moving towards the bump center in the streamwise x -direction, see figure 13. The corresponding grid resolution is $\Delta x^+ = 15 \div 72$, $\Delta y_{wall}^+ = 2.5 \div 5$ and $\Delta z^+ = 30$. On the other hand, the coarser mesh is composed of $0.5M$ cells and the grid resolution is $\Delta x^+ = 60 \div 115$, $\Delta y_{wall}^+ = 10 \div 20$ and $\Delta z^+ = 30$. The wall-normal resolution for the coarser mesh has been intentionally designed to be coarse enough to address also the dynamic RANS performances when coupled with wall functions. Indeed, the T-Flows solver makes use of an elliptical blending function that, depending on the distance from the wall of the first cell, progressively activates the wall function required for very-coarse grained simulations of the near-wall region. In particular, the blending function for the coarse mesh leads approximately to 60% of usage of the wall function among the whole domain while for the finer mesh to 0% of usage meaning that no wall function is used.

We start the analysis of the results by addressing the instantaneous flow solution. As shown in figure 14, the dynamic RANS formalism is found again to provide many insights about the 3D and unsteady turbulent phenomena characterizing the flow solution. Although not reported for brevity reasons, the standard $k - \varepsilon$ implementation lacks in capturing this physics by reproducing a steady 2D flow pattern. Hence, the ability of the dynamic RANS approach in enabling scale-resolving features that are supported by the grid resolution is confirmed also in the fully turbulent conditions provided by the flow over a bump. The solution of the dynamic RANS formalism remains turbulent also when coarsening the grid with the only difference being the absence of fine-scale structures not supported by the spatial resolution, see again figure 14. Notice that in the coarse grid simulation wall functions are also widely adopted. Hence, the ability of the dynamic procedure in smoothly transitioning to a very-coarse modelling approach is further confirmed also by the flow over a bump.

From a more quantitative point of view, we analyse first the statistical features of the recirculating bubble generated by the bump. As shown in table 2, the average position of the flow separation x_s is nicely captured by the dynamic procedure compared to DNS data (Mollicone *et al.* 2017) for both the fine and coarse simulations. On the contrary, the standard $k - \varepsilon$ approach significantly fails in predicting the phenomenon of separation especially in the coarse simulation. Contrary to the dynamic RANS formalism, the standard $k - \varepsilon$ model is not able to capture the damping of turbulence induced by the

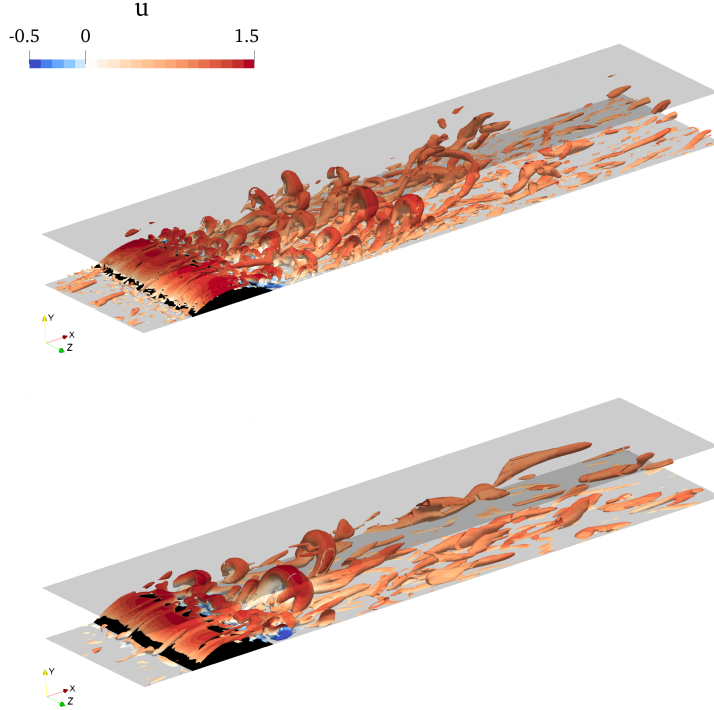


FIGURE 14. Turbulent flow over a bump. Instantaneous flow realizations reported with iso-surfaces the Q-Criterion (Hunt *et al.* 1988), $Q = 0.15$, colored with streamwise velocity. Solution of the dynamic RANS approach for the fine mesh (top) and for the coarse mesh (bottom).

	x_s	x_r	c_d
DNS (Mollicone <i>et al.</i>)	4.4	6.2	$2.05 \cdot 10^{-2}$
Dyn. $k - \varepsilon$ (fine)	4.4	6.6	$2.04 \cdot 10^{-2}$
Dyn. $k - \varepsilon$ (coarse)	4.6	7	$1.84 \cdot 10^{-2}$
$k - \varepsilon$ (fine)	4.9	6.2	$1.93 \cdot 10^{-2}$
$k - \varepsilon$ (coarse)	5.5	6.1	$1.61 \cdot 10^{-2}$

TABLE 2. Streamwise position of the mean flow separation x_s and reattachment x_r and drag coefficient c_d .

favorable pressure gradient in the windward side of the bump thus drastically delaying the point of separation. For the same reason, a shrinking of the size of the separation bubble is predicted by the standard $k - \varepsilon$ solution. Indeed, the reattachment length x_r is only slightly overestimated by the dynamic RANS approach but not by the standard $k - \varepsilon$ solution, see again table 2. The behaviour of the flow separation and reattachment drastically influences the overall drag coefficient of the flow. As shown in table 2, the predicted drag coefficient is indeed improved by the dynamic RANS approach compared with the standard $k - \varepsilon$ solution.

The mean streamwise velocity profiles obtained with the fine grid simulations of the dynamic RANS and standard $k - \varepsilon$ approaches are shown in figure 15 compared with those of the DNS by Mollicone *et al.* (2017). The profiles are reported for relevant streamwise

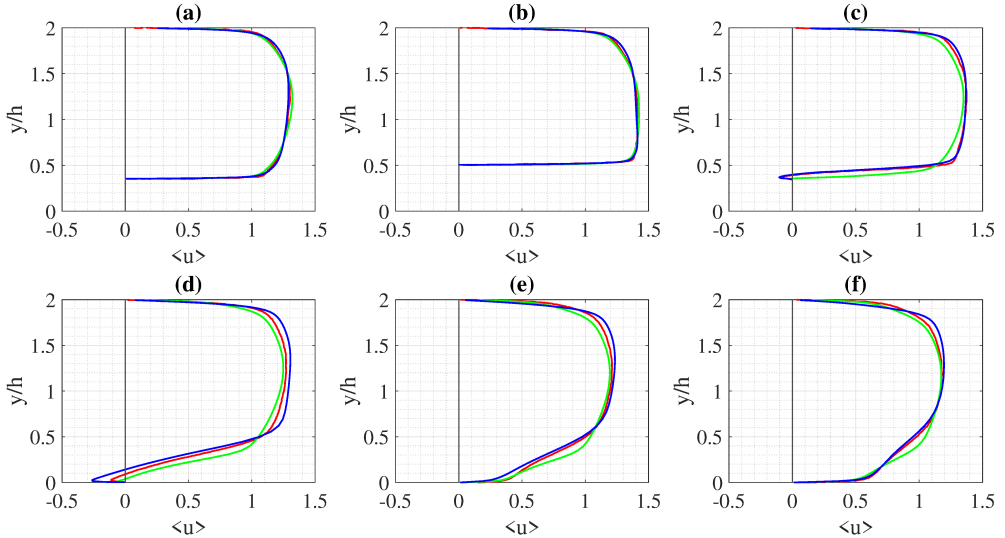


FIGURE 15. Turbulent flow over a bump. Mean streamwise velocity profiles at different streamwise positions (a), (b), (c), (d), (e) and (f) reported in figure 13. Finer grid solutions of the dynamic RANS (blue line) and standard $k-\varepsilon$ (green line) are compared with DNS data (Mollicone *et al.* 2017) (red line).

flow positions starting from the windward side of the bump and ending in the reattached flow region as highlighted with letters from *a* to *f* in figure 13. The DNS behaviour is well reproduced by the dynamic RANS solution. Compared with the standard $k-\varepsilon$ approach, a significant improvement is observed especially at streamwise positions corresponding to the recirculating bubble and to the downstream flow development (streamwise positions *c-f*). This improvement supports the idea that the dynamic RANS approach outperforms the standard $k-\varepsilon$ model in predicting the turbulence weakening induced by favorable pressure gradients in the windward side of the bump with obvious repercussions for the downstream development of the solution. Roughly the same improvement is observed when coarsening the grid although these results are not reported here for the sake of brevity.

The streamwise velocity variance profiles obtained with the fine grid simulations of the dynamic RANS and standard $k-\varepsilon$ approaches are shown in figure 16. The reference solution provided by the DNS of Mollicone *et al.* (2017) is nicely captured by the dynamic RANS formalism. In particular, the shape of the streamwise velocity variance profiles, the positions of their peaks and also their intensity conform with those of the DNS thus further proving the quality of the dynamic RANS solution and of its capability in capturing the relevant physics of the flow. This physics is completely missed by the standard $k-\varepsilon$ approach that indeed reproduces a steady 2D solution.

REFERENCES

BASSI, F., BOTTI, L., COLOMBO, A., CRIVELLINI, A., FRANCIOLINI, M., GHIDONI, A. & NOVENTA, G. 2020 A p-adaptive matrix-free discontinuous galerkin method for the implicit les of incompressible transitional flows. *Flow, Turbulence and Combustion* **105**, 437–470.

BRUNO, L., SALVETTI, M. V. & RICCIARDELLI, F. 2014 Benchmark on the aerodynamics of a rectangular 5:1 cylinder: an overview after the first four years of activity. *J. Wind Eng. Ind. Aerodyn.* **126**, 87–106.

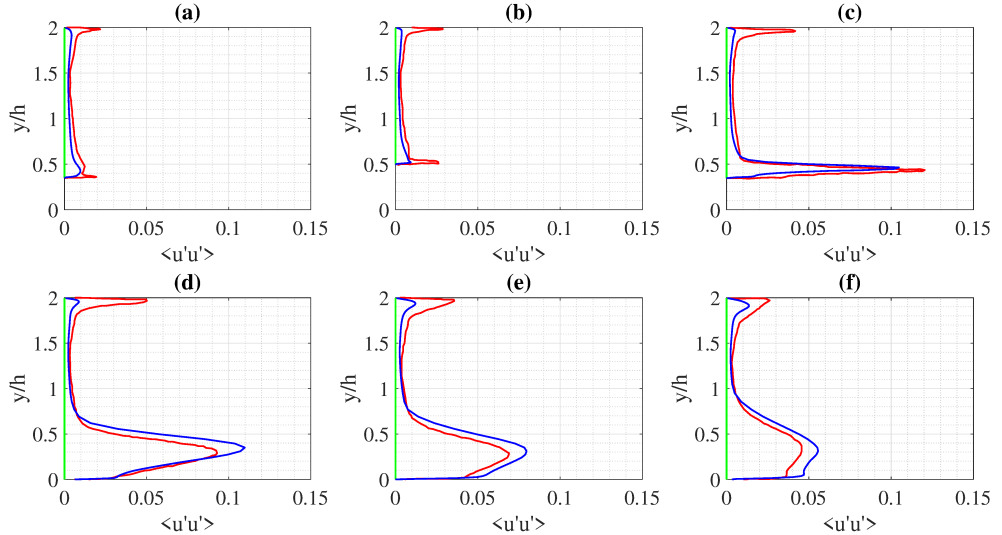


FIGURE 16. Turbulent flow over a bump. Streamwise velocity variance profiles at different streamwise positions (a), (b), (c), (d), (e) and (f) reported in figure 13. Finer grid solutions of the dynamic RANS (blue line) and standard $k - \varepsilon$ (green line) are compared with DNS data (Mollicone et al. 2017) (red line).

CHIARINI, A. & QUADRO, M. 2021 The turbulent flow over the barc rectangular cylinder: A dns study. *Flow, Turbulence and Combustion* **107**, 875–899.

CIMARELLI, A., CORSINI, R. & STALIO, E. 2024 Reynolds number effects in separating and reattaching flows with passive scalar transport. *J. Fluid Mech.* **984**, A20.

CIMARELLI, A., FRANCIOLINI, M. & CRIVELLINI, A. 2020 Numerical experiments in separating and reattaching flows. *Phys. Fluids* **32** (9).

CIMARELLI, A., LEONFORTE, A. & ANGELI, D. 2018 On the structure of the self-sustaining cycle in separating and reattaching flows. *J. Fluid Mech.* **857**, 907–936.

CRIVELLINI, A., NIGRO, A., COLOMBO, A., GHIDONI, A., NOVENTA, G., CIMARELLI, A. & CORSINI, R. 2022 Implicit large eddy simulations of a rectangular 5:1 cylinder with a high-order discontinuous galerkin method. *Wind and Structures* **34**, 59–72.

DELIBRA, G., HANJALIĆ, K., BORELLO, D. & RISPOLI, F. 2010 Vortex structures and heat transfer in a wall-bounded pin matrix: LES with a RANS wall-treatment. *Int. J. Heat Fluid Flow* **31** (5), 740–753.

DUFFAL, V., DE LAAGE DE MEUX, B. & MANCEAU, R. 2022 Development and validation of a new formulation of hybrid temporal large eddy simulation. *Flow, Turb. and Comb.* **108** (1), 1–42.

FADAI-GHOTBI, A., FRIESS, C., MANCEAU, R., GATSKI, T. B. & BORÉE, J. 2010 Temporal filtering: A consistent formalism for seamless hybrid RANS–LES modeling in inhomogeneous turbulence. *Int. J. Heat Fluid Flow* **31** (3), 378–389.

FRIESS, C., MANCEAU, R. & GATSKI, T. B. 2015 Toward an equivalence criterion for hybrid RANS/LES methods. *Computers & Fluids* **122**, 233–246.

FRÖHLICH, J. & VON TERZI, D. 2008 Hybrid LES/RANS methods for the simulation of turbulent flows. *Progress in Aerospace Sciences* **44** (5), 349–377.

GASKELL, P. H. & LAU, A. K. C. 1988 Curvature-compensated convective transport: Smart, a new boundedness-preserving transport algorithm. *International Journal for Numerical Methods in Fluids* **8**, 617–641.

GERMANO, M. 1992 Turbulence: the filtering approach. *J. Fluid Mech.* **238**, 325–336.

GERMANO, M., PIOMELLI, U., MOIN, P. & CABOT, W. H. 1991 A dynamic subgrid-scale eddy viscosity model. *Phys. Fluids* **3** (7), 1760–1765.

HADŽIABDIĆ, M., HAFIZOVIĆ, M., NIČENO, B. & HANJALIĆ, K. 2022 A rational hybrid RANS-

LES model for cfd predictions of microclimate and environmental quality in real urban structures. *Building and Environment* **217**, 109042.

HANJALIĆ, K., POPOVAC, M & HADŽIABDIĆ, M 2004 A robust near-wall elliptic-relaxation eddy-viscosity turbulence model for cfd. *Int. J. Heat and Fluid Flow* **25** (6), 1047–1051.

HUNT, J. CR, WRAY, A. A. & MOIN, P 1988 Eddies, streams, and convergence zones in turbulent flows. *Center for Turbulence Research Report CTR-S88*, 193.

KAMPÉ DE FÉRIET, J. & BETCHOV, R. 1951 Theoretical and experimental averages of turbulent functions. In *Proc. K. Ned. Akad. Wet.*, , vol. 53, pp. 389–398.

KLEIN, M. & GERMANO, M. 2020 Analysis and modelling of the commutation error. *Fluids* **6** (1), 15.

LAUNDER, B.E. & SPALDING, D.B. 1983 The numerical computation of turbulent flows. In *Numerical prediction of flow, heat transfer, turbulence and combustion*, pp. 96–116. Elsevier.

LEONARD, A. 1975 Energy cascade in large-eddy simulations of turbulent fluid flows. *Adv. in geophysics* **18**, 237–248.

LILLY, D.K. 1992 A proposed modification of the Germano subgrid-scale closure method. *Phys. Fluids A* **4**, 633–635.

MANNINI, C., SCHEWE, G. & ŠODA, A. 2010 Unsteady rans modelling of flow past a rectangular cylinder: Investigation of reynolds number effects. *Computers & Fluids* **39**, 1609–1624.

MENEVEAU, C. & KATZ, J. 2000 Scale-invariance and turbulence models for large-eddy simulation. *Annual Review of Fluid Mechanics* **32** (1), 1–32.

MOLLICONE, J.-P., BATTISTA, F., GUALTIERI, P. & CASCIOLO, C. M. 2017 Effect of geometry and reynolds number on the turbulent separated flow behind a bulge in a channel. *Journal of Fluid Mechanics* **823**, 100–133.

PRUETT, C. 2008 Temporal large-eddy simulation: theory and implementation. *Theor. Comput. Fluid Dyn.* **22**, 275–304.

PRUETT, C.D., GATSKI, T.B., GROSCH, C.E. & THACKER, W.D. 2003 The temporally filtered navier–stokes equations: properties of the residual stress. *Phys. Fluids* **15** (8), 2127–2140.

SPALART, P. R. 2021 Hybrid RANS-LES methods. In *Advanced Approaches in Turbulence*, pp. 133–159. Elsevier.

WILCOX, DAVID C & OTHERS 1998 *Turbulence modeling for CFD*, , vol. 2. DCW industries La Canada, CA.

WORNON, S., OUVRARD, H., SALVETTI, M. V., KOOBUS, B. & DERVIEUX, A. 2011 Variational multiscale large-eddy simulations of the flow past a circular cylinder: Reynolds number effects. *Computers & Fluids* **47** (1), 44–50.

YANG, Z. & VOKE, P. R. 2001 Large-eddy simulation of boundary-layer separation and transition at a change of surface curvature. *J. Fluid Mech.* **439**, 305–333.

YIN, Z., REDDY, K. R. & DURBIN, P. A. 2015 On the dynamic computation of the model constant in delayed detached eddy simulation. *Phys. Fluids* **27** (2).